Full-scale solutions to particle-laden flows: Multidirect forcing and immersed boundary method

Kun Luo, Zeli Wang, Jianren Fan,* and Kefa Cen
State Key Laboratory of Clean Energy Utilization, Zhejiang University, Hangzhou 310027, People's Republic of China
(Received 7 March 2007; revised manuscript received 13 June 2007; published 27 December 2007)

Towards getting the full-scale solutions to particle-laden flows, a multidirect forcing technique and immersed boundary method are proposed in the present work. The immersed solid boundary is represented by Lagrangian points and the no-slip condition is efficiently satisfied by exerting multidirect forcing. The hydrodynamic interactions between the stationary or moving solid boundary and the Newtonian fluid are able to be accurately described. This method is simple but efficient which is validated by simulating the flows around a stationary circular disc at different Reynolds numbers and the free sedimentation of a particle. The predicted results agree well with previous experimental and numerical data. When applying this method to study particle sedimentation near a vertical wall, the rotation shifting phenomenon is observed besides the anomalous rolling and the lateral migration.

DOI: 10.1103/PhysRevE.76.066709 PACS number(s): 47.55.Kf, 47.27.ek, 47.61.Jd

I. INTRODUCTION

Particle-laden flows exist widely both in nature and in engineering application systems, such as drop of rain droplet in air, sedimentation of aerosol in atmosphere, snow and dust storms, as well as powder transport, spray combustion, and gas-solid or liquid-solid fluidized beds, and many more. Because of its great importance, the problem has attracted both physicists and engineers to develop reliable theory and model to predict the motions of dispersed particles in various flows [1–3].

Traditionally, the theoretical analysis or numerical simulation of particle-laden flows is mainly based on the assumption that the particle size is small enough, thus the particle can be regarded as a mass point and the effects of particle size on the flows are neglected. This assumption is available for so many cases that it has been extensively applied in numerous studies in the past decades [4–8]. Even in the traditional direct numerical simulation (DNS) of multiphase flows, the point-particle assumption is also used and the force is often modeled by Stokes or modified drag law. However, this assumption is invalid in some conditions where the particle volume is dominant, such as slurries, fluidized beds, sedimentations, and suspensions.

To overcome this problem, various modern DNS methods have been developed in the recent 15 years. In modern DNS methods, the particle is considered as real finite volume and the hydrodynamic interactions are accurately calculated by integrating the viscosity and pressure forces imposed by surrounding fluid. No empirical model is introduced and the fine structures around the particles can also be captured. From this point of view, this level DNS is the fully resolved or DNS of multiphase flows with full-scale solutions. Hu and co-workers [9,10] proposed the boundary fitted techniques based on unstructured and adapting mesh to simulate fluid-particle motions. To avoid the time-consuming remeshing, a series of methods based on fixed Cartesian grid were also put forward. Ladd [11,12] successfully applied the lattice Boltzmann method (LBM) to simulate particle-fluid suspensions. Kalthoff *et al.* [13] proposed the method that incorporates analytical solutions for the region near the particle surface, with some parameters determined by matching the outer flow conditions. Glowinski *et al.* [14] presented a distributed Lagrange multiplier–fictitious domain method (DLM-FD) for particulate flows. Kuttech [15] presented the Stokesian dynamics simulation (SDS) method to study the properties of suspensions of nonspherical particles. For liquid-liquid or gas-liquid two-phase flows, the level set method [16] and the front tracking method [17] have also been presented.

Especially, the immersed boundary method (IB method), originally developed by Peskin [18], has attracted considerable interest recently [19]. In the IB method, the solid boundaries immersed in the fluid are normally represented by a set of Lagrangian boundary points that are advected by the fluid-solid interactions. Goldstein *et al.* [20] used the so-called adaptive or feedback forcing scheme to model the no-slip conditions on a stationary boundary. This technique necessitates the use of two free parameters that must be chosen, based on the flow conditions. Hofler and Schwarzer [21] presented a finite-difference method for particle-laden flows by adding a constraint force into the Navier-Stokes equations to enforce rigid particle motions, with the constraint force being determined by a penalty method. Kajishima [22] investigated the particulate flows interactions via introducing the volume-weighted average velocity close to the solid-fluid interface. Nakayama and Yamamoto [23] presented a modified computational method to resolve hydrodynamic interactions in colloidal dispersions. The boundaries between solid particles and fluid are replaced with a continuous interface by assuming a smoothed profile. Yang and Mao [24] presented a mirror fluid method for simulating solid-fluid two-phase flow. The boundary condition is enforced implicitly on solid-fluid surface segments by mirror relations. Different from the above methods, Fadlun *et al.* [25] introduced direct forcing [26] to calculate the interactions between immersed boundary and fluid. The velocity at the points which are close to the immersed boundary is simply set at every time step. It looks like applying an equivalent forcing term to the Navier-Stokes equations. Compared with the feedback forcing, the direct forcing IB method is more general because the com-

*Corresponding author. fanjr@zju.edu.cn

putation no longer suffers the stability limitation and no empirical constants are needed as in Goldstein *et al.*'s [20] scheme. However, the formulation of direct forcing is based on a single Lagrangian point and when applying direct forcing to a group of interactional Lagrangian points, the velocity on the Lagrangian point at the immersed boundary may not effectively satisfy the no-slip boundary condition due to the mutual influence of the direct forcing at the neighboring points through the interpolation or extrapolation scheme or the Dirac delta function, which is also one of the greatest challenges in the above modern DNS methods for particle-laden flows with full-scale solutions.

Towards the DNS of particle-laden flows with full-scale solutions, an improved IB method, the multidirect forcing IB method is presented in the study based on the basic idea of direct forcing [25,26]. The difference from previous direct-forcing methods is in the multiple application of direct forcing to obtain the better result. By using this method, the velocity at the immersed boundary is able to satisfy the no-slip boundary condition immediately and accurately. It is validated by simulating the flow around a circular disc and the free sedimentation of a particle. The method is also extended to investigate particle sedimentation near a vertical wall. Some microcosmic phenomena are successfully observed.

The paper is organized as follows. Section II is the numerical method which includes the governing equations, the basic formation of direct forcing, and the proposed multidirect forcing scheme. The validations of the multidirect forcing scheme are demonstrated in Sec. III. Section IV is about the application to particle sedimentation near a vertical wall and Sec. V is devoted to the summary.

II. NUMERICAL METHOD

A. Governing equations

Consider a flow comprised of viscous incompressible fluid immersed with dispersed particles. The nondimensional governing equations for the fluid read

$$\nabla \cdot \boldsymbol{u} = 0, \tag{1}$$

$$\frac{\partial \boldsymbol{u}}{\partial t} + \boldsymbol{u} \cdot \nabla \boldsymbol{u} = -\nabla P + \frac{1}{\mathrm{Re}} \nabla^2 \boldsymbol{u} + \boldsymbol{f}, \tag{2}$$

where $\boldsymbol{u}$ is the velocity of fluid, P is the pressure, Re is the Reynolds number, and $\boldsymbol{f}$ is the body force exerted on the fluid by the immersed particles and will be described in detail in the following, Secs. II B and II C sections. These equations are enforced throughout the entire computational domain Ω, comprising the actual fluid domain Ω_f and the space Ω_p occupied by N_p immersed solid particles.

In order to impose the restrained conditions on the space Ω_p occupied by particles, one needs to describe the motion of the immersed particles under the action of gravity and hydrodynamic forces. The motion of a solid particle is governed by Newton's equations for the linear, angular momentum, and transportation of a rigid body as follows:

$$\frac{d(m_p \boldsymbol{v}_\mathrm{c})}{dt} = \boldsymbol{F} + \boldsymbol{g}_p, \tag{3}$$

$$\frac{d\boldsymbol{x}_\mathrm{c}}{dt} = \boldsymbol{v}_\mathrm{c}, \tag{4}$$

$$\frac{d(\boldsymbol{I}_p \cdot \boldsymbol{\omega}_p)}{dt} = \boldsymbol{T}, \tag{5}$$

$$\frac{d\boldsymbol{\theta}_\mathrm{p}}{dt} = \boldsymbol{\omega}_\mathrm{p}, \tag{6}$$

where m_p, $\boldsymbol{v}_\mathrm{c}$, $\boldsymbol{x}_\mathrm{c}$, $\boldsymbol{I}_p$, $\boldsymbol{\omega}_p$, $\boldsymbol{\theta}_p$ are the mass, the velocity of the center of mass, the position of the center of mass, the inertia tensor, the angular velocity, and the angular orientation of the particle; $\boldsymbol{F}$ and $\boldsymbol{T}$ represent the hydrodynamic force and torque acting upon the particle by the fluid; $\boldsymbol{g}_p$ is the gravity force.

To solve the above governing equations, the spatial derivatives are discretized using the fourth-order compact finite difference scheme [27] and the four-step-four-order Runge-Kutta marching scheme [28] is used for time integration.

B. Direct forcing scheme

In IB methods, the fixed Cartesian coordinates and the discretized Lagrangian points uniformly distributed over the immersed boundary are often used. In the direct forcing scheme [25,26], for the Lagrangian point $\boldsymbol{x}_k$ at the immersed boundary, a forcing $\boldsymbol{F}_k(\boldsymbol{x}_k)$ is imposed to make the local velocity obtained from Eulerian location equal to the desired velocity, i.e., the actual velocity of the Lagrangian point at the immersed boundary $\boldsymbol{u}_p = \boldsymbol{v}_\mathrm{c} + \boldsymbol{\omega}_\mathrm{p}(\boldsymbol{x}_k - \boldsymbol{x}_\mathrm{c})$, which can let the velocity on the Lagrangian point satisfy the no-slip boundary condition. The forcing $\boldsymbol{F}_k(\boldsymbol{x}_k)$ can be determined as follows.

From Eq. (2), one can get

$$\boldsymbol{f} = \frac{\partial \boldsymbol{u}}{\partial t} + \boldsymbol{u} \cdot \nabla \boldsymbol{u} + \nabla P - \frac{1}{\mathrm{Re}} \nabla^2 \boldsymbol{u} = \frac{\partial \boldsymbol{u}}{\partial t} + \boldsymbol{R} = \frac{\boldsymbol{u}^{\mathrm{n}+1} - \boldsymbol{u}^{\mathrm{n}}}{\Delta t} + \boldsymbol{R}, \tag{7}$$

where n represents the time level and $\boldsymbol{R} = \boldsymbol{u} \cdot \nabla \boldsymbol{u} + \nabla P - \frac{1}{\mathrm{Re}} \nabla^2 \boldsymbol{u}$. Then

$$\boldsymbol{F}_k(\boldsymbol{x}_k) = \frac{\boldsymbol{u}_\mathrm{k}^{\mathrm{n}+1} - \boldsymbol{u}_\mathrm{k}^{\mathrm{n}}}{\Delta t} + \boldsymbol{R} = \frac{\boldsymbol{u}_\mathrm{k}^{\mathrm{n}+1} - \hat{\boldsymbol{u}}_\mathrm{k}}{\Delta t} + \frac{\hat{\boldsymbol{u}}_\mathrm{k} - \boldsymbol{u}_\mathrm{k}^{n}}{\Delta t} + \boldsymbol{R} = \frac{\boldsymbol{u}_\mathrm{p}^{\mathrm{n}+1} - \hat{\boldsymbol{u}}_\mathrm{k}}{\Delta t}, \tag{8}$$

where $\hat{\boldsymbol{u}}_k$ is a temporary velocity which satisfies the momentum equation, that is,

$$\frac{\hat{\boldsymbol{u}}_\mathrm{k} - \boldsymbol{u}_\mathrm{k}^{\mathrm{n}}}{\Delta t} + \boldsymbol{R} = 0. \tag{9}$$

Under the effect of the forcing, the velocity on the Lagrangian point $\boldsymbol{x}_k$ at the $n+1$ time level $\boldsymbol{u}_\mathrm{k}^{\mathrm{n}+1}$ can be modified

to the desired velocity $\boldsymbol{u}_p^{\mathrm{n+1}}$. The forcing is direct in the sense that the desired value of velocity is imposed directly on the boundary without any dynamical process [25] and the forcing is based upon the law of conservation [29].

To spread the quantities between Eulerian grids and Lagrangian points, the discrete delta function provided by Griffith and Peskin [30] is applied in the present study. The temporary velocity on the Lagrangian point at the immersed boundary $\boldsymbol{x}_k$ is obtained from its surrounding Eulerian grids $\boldsymbol{x}$,

$$\hat{\boldsymbol{u}}_k = \sum_{\boldsymbol{x}\in\Omega} \hat{\boldsymbol{u}} \cdot \delta_h(\boldsymbol{x}_k - \boldsymbol{x}) \cdot h^2, \tag{10}$$

where $\hat{\boldsymbol{u}}$ is the temporary velocity on the Eulerian grids which satisfies Eq. (9) and

$$\delta_h(\boldsymbol{x} - \boldsymbol{x}_k) = \frac{1}{h^2} d_h\left(\frac{x - x_k}{h}\right) d_h\left(\frac{y - y_k}{h}\right), \tag{11}$$

where $\boldsymbol{x}=(x,y)$, $\boldsymbol{x}_k=(x_k,y_k)$, h is the Eulerian mesh size, and

$$d_h(r) = \begin{cases} \frac{1}{8}(3 - 2|r| + \sqrt{1 + 4|r| - 4r^2}) & 0 \le |r| < 1 \\ \frac{1}{8}(5 - 2|r| - \sqrt{-7 + 12|r| - 4r^2}) & 1 \le |r| < 2 \\ 0 & 2 \le |r|. \end{cases} \tag{12}$$

Thus the body force in Eq. (2) or the effect of the forcing on the Lagrangian points spreading into the Eulerian grids $\boldsymbol{f}$ can be expressed as

$$\boldsymbol{f} = \int \boldsymbol{F}_k(\boldsymbol{x}_k) \cdot \delta(\boldsymbol{x} - \boldsymbol{x}_k) d\boldsymbol{x}_k = \sum_{\mathrm{k}=1}^{N} \boldsymbol{F}_k(\boldsymbol{x}_k) \cdot \delta_h(\boldsymbol{x} - \boldsymbol{x}_k) \cdot \Delta V_k, \tag{13}$$

where N is the number of the Lagrangian points set at the immersed boundary and ΔV_k is the discrete volume for each Lagrangian point [31].

Based on the above direct-forcing scheme and immersed boundary method, the hydrodynamic force and the torque exerted on a moving particle can be expressed as

$$\boldsymbol{F} = -\int_1^N \boldsymbol{F}_k(\boldsymbol{x}_k) d\boldsymbol{s} = -\int_\Omega \boldsymbol{f}(\boldsymbol{x}) d\boldsymbol{x} = -\sum_{\boldsymbol{x}\in\Omega} \boldsymbol{f}(\boldsymbol{x}) h^2, \tag{14}$$

$$\begin{aligned} \boldsymbol{T} &= -\int_1^N (\boldsymbol{x}_k - \boldsymbol{x}_c) \times \boldsymbol{F}_k(\boldsymbol{x}_k) d\boldsymbol{s} \\ &= -\int_\Omega (\boldsymbol{x} - \boldsymbol{x}_c) \times \boldsymbol{f}(\boldsymbol{x}) d\boldsymbol{x} \\ &= -\sum_{\boldsymbol{x}\in\Omega} (\boldsymbol{x} - \boldsymbol{x}_c) \times \boldsymbol{f}(\boldsymbol{x}) h^2. \end{aligned} \tag{15}$$

When spreading the effect of the forcing from Lagrangian points to Eulerian nodes with the direct forcing scheme, the force acted on the Lagrangian point which contains the desired velocity $\boldsymbol{u}_p^{n+1}$ should be calculated by using Eq. (8). However, the desired velocity at $n+1$ time level $\boldsymbol{u}_p^{n+1}$ is unknown. A simple way to deal with it is applying a one-order explicit scheme with $\boldsymbol{u}_{\mathrm{p}}^{\mathrm{n}}$ instead of $\boldsymbol{u}_{\mathrm{p}}^{\mathrm{n+1}}$ [22]. For the sake of convenience, we also use this explicit scheme in the present study. Then the force exerted on the Lagrangian point at the immersed boundary should be changed as

$$\boldsymbol{F}_k(\boldsymbol{x}_k) = \frac{\boldsymbol{u}_{\mathrm{p}}^{\mathrm{n+1}} - \hat{\boldsymbol{u}}_{\mathrm{k}}}{\Delta t} \approx \frac{\boldsymbol{u}_{\mathrm{p}}^{\mathrm{n}} - \hat{\boldsymbol{u}}_{\mathrm{k}}}{\Delta t}. \tag{16}$$

C. Multidirect forcing scheme

The above direct forcing exerted on the Lagrangian point $\boldsymbol{x}_k$ can gradually modify the computational velocity $\hat{\boldsymbol{u}}_k$ to the desired velocity $\boldsymbol{u}_p$. However, when spreading the effect of forcing from the Lagrangian points to the Eulerian grids, different schemes of discrete delta function can lead to different results, as demonstrated by Griffith and Peskin [30]. Furthermore, the velocities on the Lagrangian points may not satisfy the no-slip boundary condition very well during the process of interpolation to obtain the simulated velocity on the Lagrangian points and extrapolation to spread the forcing effect to its surrounding Eulerian grids. Therefore a multidirect forcing technique is proposed and described below.

By solving the above equations, one can get the velocity of the whole flow field $\boldsymbol{u}_1^{\mathrm{n+1}}$ where $n+1$ is the time level and the subscript 1 represents exerting the direct forcing for the first time. Then the velocity on the Lagrangian point is

$$\hat{\boldsymbol{u}}_{\mathrm{k}}^1 = \sum \boldsymbol{u}_1^{\mathrm{n+1}} \cdot \delta(\boldsymbol{x}_k - \boldsymbol{x}) \cdot h^2. \tag{17}$$

The best result is $\hat{\boldsymbol{u}}_{\mathrm{k}}^1 = \boldsymbol{u}_p$, but always $\hat{\boldsymbol{u}}_{\mathrm{k}}^1 \neq \boldsymbol{u}_p$. Although the velocity at the immersed boundary can get very close to the desired velocity after a long period of time, the no-slip boundary condition is still not satisfied very well. This situation can be changed by applying the direct forcing for the second time which makes

$$\boldsymbol{F}_{\mathrm{k}}^2(\boldsymbol{x}_k) = \frac{\boldsymbol{u}_{\mathrm{p}} - \hat{\boldsymbol{u}}_{\mathrm{k}}^1}{\Delta t}. \tag{18}$$

Then the forcing spreads from Lagrangian points to Eulerian grids through the Dirac-delta function

$$\boldsymbol{f}^2 = \sum_{\mathrm{k}=1}^{N} \boldsymbol{F}_{\mathrm{k}}^2(\boldsymbol{x}_k) \cdot \delta(\boldsymbol{x} - \boldsymbol{x}_k) \cdot \Delta V_k. \tag{19}$$

After exerting the direct forcing for the second time, the velocity of the whole flow field becomes

$$\boldsymbol{u}_2^{\mathrm{n+1}} = \boldsymbol{u}_1^{\mathrm{n+1}} + \boldsymbol{f}^2 \cdot \Delta t. \tag{20}$$

Thus the velocity on the Lagrangian point at the immersed boundary becomes

$$\hat{\boldsymbol{u}}_{\mathrm{k}}^2 = \sum \boldsymbol{u}_2^{\mathrm{n+1}} \cdot \delta(\boldsymbol{x}_k - \boldsymbol{x}) \cdot h^2. \tag{21}$$

The value of $\hat{\boldsymbol{u}}_{\mathrm{k}}^2$ is expected to be closer to the desired velocity $\boldsymbol{u}_{\mathrm{p}}$ than that of $\hat{\boldsymbol{u}}_{\mathrm{k}}^1$. The velocity at the immersed boundary can get very close to the desired velocity after this procedure is applied several times during one time step. The

total force exerting on each Lagrangian point $F_k(\boldsymbol{x}_k)$ is the sum of the forcing exerting on each Lagrangian point for the whole m times, that is

$$\boldsymbol{F}_k(\boldsymbol{x}_k) = \sum_{i=1}^{m} \boldsymbol{F}_k^i(\boldsymbol{x}_k). \tag{22}$$

Then the body force in Eq. (2), $\boldsymbol{f}$, can be expressed as

$$\boldsymbol{f} = \int \boldsymbol{F}_k(\boldsymbol{x}_k) \cdot \delta(\boldsymbol{x} - \boldsymbol{x}_k) d\boldsymbol{x}_k = \sum_{\mathrm{k}=1}^{N} \left(\sum_{i=1}^{m} \boldsymbol{F}_k^i(\boldsymbol{x}_k) \right) \cdot \delta_h(\boldsymbol{x} - \boldsymbol{x}_k) \cdot \Delta V_k. \tag{23}$$

This multidirect forcing scheme faces the fact that the formulation of direct forcing is based on a single Lagrangian point and when applying direct forcing on a group of interactional Lagrangian points and spreading the effect of forcing to Eulerian grids through the interpolation-extrapolation scheme or the Dirac delta function, the direct forcing will not be so effective. It can be seem as an explicit iterative process and the multiple applying direct forcing is different from the previous direct forcing schemes [25,26,30,31] in which the direct forcing is applied only once in one time step.

III. VALIDATION OF THE MULTIDIRECT FORCING SCHEME

A. Flow around a stationary circular disc

To examine the response of the velocity on the immersed boundary to the time of exerting multidirect forcing, the flow around a stationary circular disc at a Reynolds number of 100 is first simulated and the l_2-norm error of the velocity on the Lagrangian point with respect to no-slip boundary condition is defined as a parameter and tracked at every time step. The l_2-norm is expressed as

$$l_2 - \mathrm{norm} = \sqrt{\frac{\sum_{k=1}^{N} [(u_k - u_p)^2 + (v_k - v_p)^2]}{N}}, \tag{24}$$

where the desired velocity at the immersed boundary is $\boldsymbol{u}_p = (u_p, v_p)$.

A rectangular computational domain is used to simulate the flow using the immersed boundary method with multidirect forcing. The number of total mesh grids is 1277×767. The characteristic length is the diameter of the circular disc and the nondimensional mesh size is $h = \frac{1}{35}$. A constant velocity profile U_∞ is specified at the inflow boundary and a nonreflecting boundary condition [32] is applied at the outflow boundary. The Neumann boundary conditions are imposed on the other boundaries. 110 Lagrangian points are uniformly distributed at the immersed boundary to ensure that the volume controlled by each Lagrangian point is not greater than that of the Eulerian grid [31]. It should be pointed out that the number of Lagrangian points in the present scheme is much less than that in Ref. [33].

Figure 1 shows the correlation between l_2-norm and the time of direct-forcing m. Here $m=1$, 2, 4, 6, 10, 20, and 50.

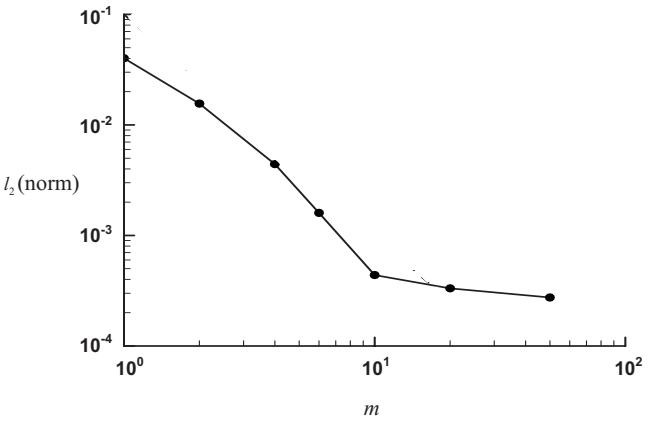

FIG. 1. Correlation between the l_2-norm and the time of multidirect forcing m.

It can be seen that as the number of m increases, the l_2-norm decreases towards zero which is the desired velocity in the simulation, i.e., $\boldsymbol{u}_p = (u_p, v_p) = (0,0)$ for the stationary circular disc. When $m=1$, the l_2-norm is 0.040 18, which means that the direct forcing has an effect on modifying the velocity at the immersed boundary to the desired velocity. However, this modifying is not satisfactory. When m increases to 20, the value of the l_2-norm decreases to 3.32×10^{-4}. This indicates that the multidirect forcing can make the velocity at the immersed boundary become closer and closer to the desired velocity and the no-slip boundary condition is able to be satisfied well. In addition, when the number of m increases from 1 to 10, the decrease of l_2-norm is faster, but when the number of m exceeds 10, the magnitude of the l_2-norm decreases slowly.

The variation of the l_2-norm with different m in the initial time framework is demonstrated in Fig. 2. As can be seen, the l_2-norm decreases to a very small value immediately with the increase of the number m, which means that the no-slip boundary condition at the immersed boundary can be satisfied in a very short time and the multidirect forcing technique is of higher efficiency.

The streamlines around the circular disc at the time $t=200$ with different times of direct forcing are shown in Fig.

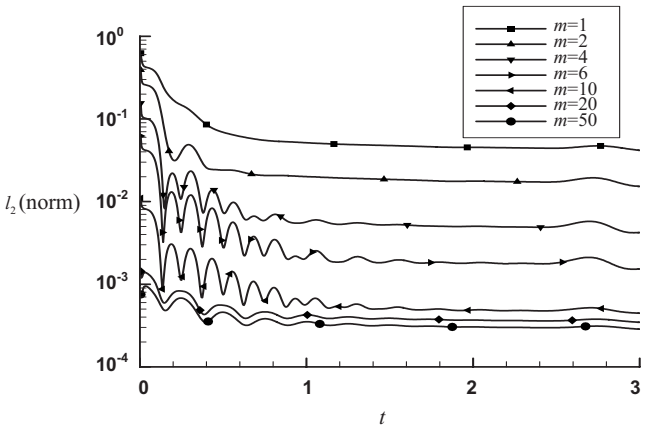

FIG. 2. Time history of the correlation between the l_2-norm and the time of multidirect forcing m in the initial time framework.

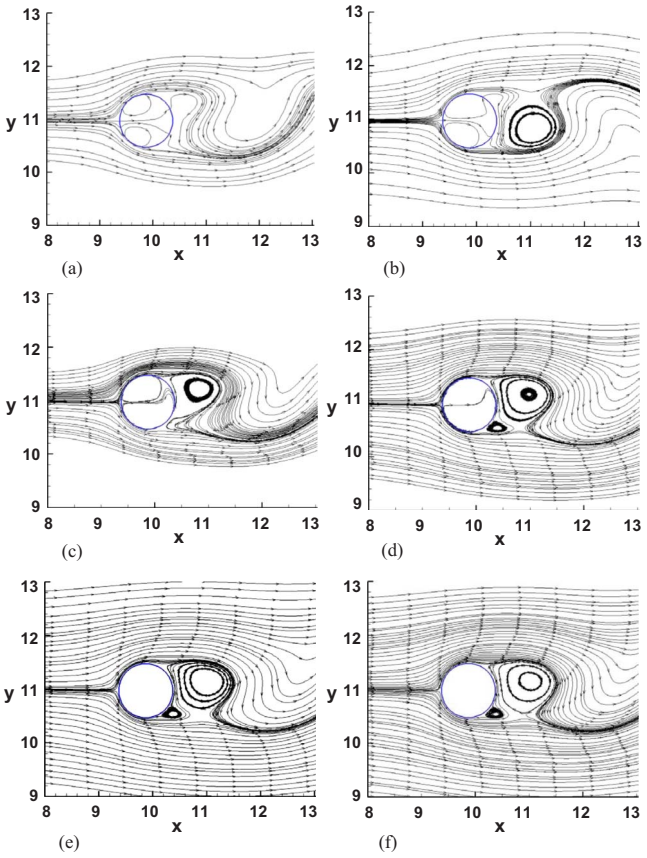

FIG. 3. (Color online) Streamlines around the circular disc at the nondimensional time $t=200$. (a) $m=1$, (b) $m=2$, (c) $m=4$, (d) $m=6$, (e) $m=10$, (f) $m=20$.

3. It is clear that the flow structures near the circular disc at $m=1$ are totally different from those at $m=20$. Because the no-slip boundary condition at the immersed boundary is satisfied inaccurately, the streamline crossing the boundary of the disc happens at $m=1$, which is obviously not physical. But when the number of m is greater than 10, there is not any streamline that can go through the boundary of the disc and the structures of flow field at $m=10$ and 20 become almost the same. This agrees well with the variation of the l_2 −norm presented in Figs. 1 and 2 and indicates that the present multidirect forcing technique can be used to simulate such complex flow with high accuracy and efficiency.

Flows past the stationary circular disc at Re=20, 40, 80, 100, and 200 are also simulated under the condition of $m=20$ and $N=110$. The predicted drag coefficient, lift coefficient, and Strouhal number are compared very well with previous experimental and numerical data [34–38]. In particular, the predicted Strouhal numbers for different Reynolds numbers are almost the same as those in the experiment of Williamson [38] as shown in Table I, which also proves the reliability of the proposed IB method with the multidirect forcing technique.

B. Free sedimentation of a particle

To further validate the multidirect forcing for simulations of a moving particle, the free sedimentation of a particle in the channel is studied. In this case, for convenience of comparison, the computational parameters are chosen as the same as those of Glowinski *et al.* [14]. The mesh sizes are set as $\frac{1}{18}$, $\frac{1}{36}$, and $\frac{1}{64}$ of the particle diameter D_p and the corresponding computational nodes are 62 785, 249 985, and 788 481, respectively. The multidirect forcing is performed for $m=20$ and 57, 114, and 202 Lagrangian points are respectively used at the immersed boundary.

The $l_{P2}-$norm error of the velocities on the Lagrangian points at the immersed boundary with respect to the no-slip boundary condition is defined as follows as a parameter and tracked at every time step:

$$l_{P2}-(\text{norm}) = \frac{\sqrt{\sum_{k=1}^{N}[(u_k-u_p)^2+(v_k-v_p)^2]/N}}{\sqrt{u_c(t)^2+v_c(t)^2+[0.5\omega(t)D_p]^2}} \quad \text{when } (u_c(t),v_c(t),\omega(t)) \neq (0,0,0) \tag{25}$$

where $u(t)=(u_c(t),v_c(t))$ is the velocity of the mass center of the particle and $\omega(t)$ is the angular velocity for the present two-dimensional flow. This $l_{P2}-$norm shows the relative error of the velocity at the immersed boundary with respect to the no-slip boundary condition.

The time history of $l_{P2}-$norm for single particle sedimentation under the conditions of $\rho_P=1.25$, $\mu=0.1$, and mesh size $h=\frac{1}{256}$ is shown in Fig. 4. The $l_{P2}-$norm decreases to 1.2×10^{-5} in a very short time and maintains this lower level during the whole simulation. This means that the multidirect forcing scheme can modify the simulated velocity at the immersed moving boundary to closely approach the desired velocity and the no-slip boundary condition can be satisfied well. Table II shows the comparison of the maximum Reynolds number defined as $\text{Re}_{\text{Max}}=\text{Max}[\text{Re}(t)]=\text{Max}[\rho_p\sqrt{u_c(t)^2+v_c(t)^2}D_p/\mu]$ during the particle settling with previous related numerical results. It can be found that the present predicted maximum Reynolds numbers under different mesh sizes are all in good agreement with those of Glowinski *et al.* [14] and Wan and Turek [39].

IV. APPLICATION TO PARTICLE SEDIMENTATION NEAR A VERTICAL WALL

Particle sedimentations in fluid under various conditions have been extensively investigated both from experiments

TABLE I. Comparison of the predicted Strouhal number with previous related data for different Reynolds numbers.

Re	Present	Xu [36]	Silva [29]	Lai [34]	Su [35]	Williamson (expt.) [38]
80	0.153		0.15		0.153	0.15
100	0.166	0.171	0.16	0.165	0.168	0.166
200	0.196	0.202		0.19		0.197

[40,41] and simulations [42–45]. Some phenomena and physics are uncovered. On a spherical particle settling near a flat wall in non-Newtonian fluid, it was found that the particle moved toward the wall and rotated as if rolling up the wall which is also being termed as "anomalous rolling" [42]. In contrast, in a Newtonian fluid at low Reynolds number, a sphere settling near a wall maintains a constant separation from it as a consequence of the reversibility of Stokes equations. The direction of rotation is always in the same sense as if the sphere were rolling along a dry wall. But if another vertical wall appears, the direction of rotation can be reversed and the anomalous rolling happens under some conditions [46,47]. In order to examine the microcosmic interactions between particle and wall, we use the multidirect forcing and immersed boundary method to get the full-scale solutions to the particle sedimentation near a vertical wall with Newtonian fluid. The computational parameters are summarized as follows.

(i) The computational domain is $\Omega=(0,2)\times(0,6)$ corresponding to a nondimensional domain $(0,8)\times(0,60)$.

(ii) The diameter of the particle is $D_P=0.25$ and the density is $\rho_P=1.5$.

(iii) The center of the particle is located at (0.2, 5) at time $t=0$ near the left one of two vertical walls.

(iv) The fluid and the particle are initially at rest.

(v) The fluid density is $\rho_f=1.00$ and the viscous is $\mu=0.01$.

(vi) The mesh size is $\frac{1}{36}$ of the particle diameter.

(vii) The evolution of velocity vector of the fluid and particle position at the initial stage of particle sedimentation is presented in Fig. 5. It can be observed that the particle settles along the vertical direction accompanied by the lateral migration away from the near wall. The vertical sedimentation and lateral migration of the spherical particle are also going with the uphill counterclockwise rotation which is also the so-called anomalous rolling [48]. These phenomena are similar to those of previous studies [46,49], but different from the particle settling near a single wall in Newtonian fluid and the particle settling near a single or two plane wall in non-Newtonian fluid. In fact, the rotation direction in the present simulation is not always counterclockwise, which will be demonstrated later. The velocity vector of the fluid shows that the fluid in front of the particle flows upward and

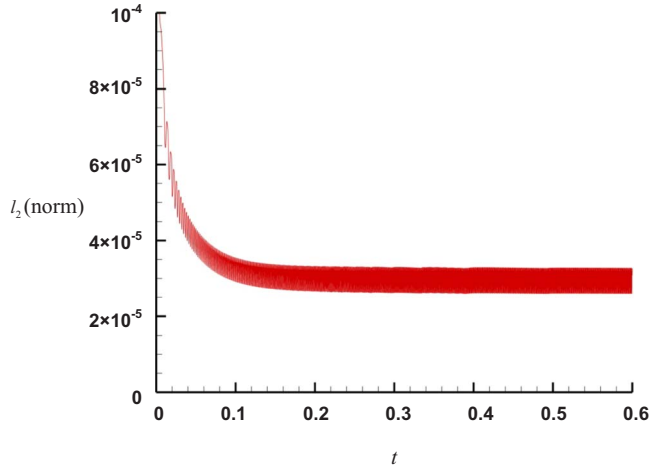

FIG. 4. (Color online) Time history of the $l_{P2}-$norm for single particle sedimentation under the condition of particle density $\rho_P=1.25$ and fluid viscosity $\mu=0.1$.

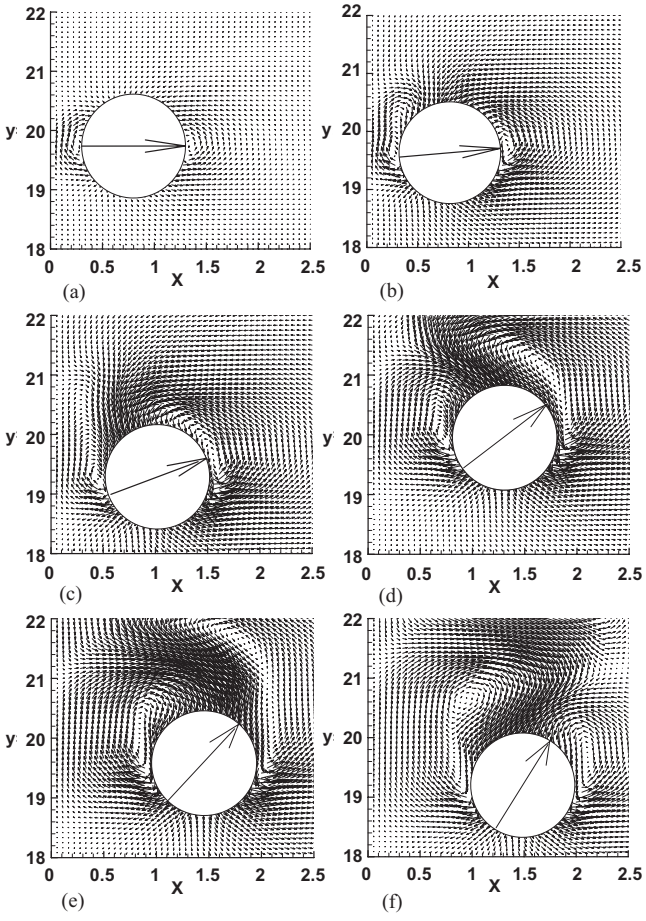

FIG. 5. Evolution of velocity vector of fluid and particle position at the initial stage of particle sedimentation under the condition of particle density $\rho_P=1.5$ and fluid viscosity $\mu=0.01$. (a) $t=0.0326$, (b) $t=0.082\,193$, (c) $t=0.122\,944$, (d) $t=0.157\,413$, (e) $t=0.189\,578$, (f) $t=0.220\,607$.

TABLE II. Comparison of the predicted maximum Reynolds number during the particle sedimentation with previous related data.

	$\rho_P=1.25$, $\mu=0.1$						
	Present			Glowinski *et al.* [14]		Wan and Turek [39]	
	$h=\frac{1}{72}$	$h=\frac{1}{144}$	$h=\frac{1}{256}$	$h=\frac{1}{192}$	$h=\frac{1}{256}$	$h=\frac{1}{48}$	$h=\frac{1}{96}$
$\mathrm{Re}_{\mathrm{Max}}$	16.96	17.22	17.32	17.27	17.31	17.42	17.15

the fluid behind the particle flows downward. Accordingly, the wake forms and sheds behind the particle. Furthermore, the velocity gradient between the near wall and the particle is larger at the beginning and then decays fast, which may impose an additional effect on particle sedimentation dynamics.

Let us examine the time history of the particle angular velocity during its sedimentation. In the very beginning time framework, the particle does not rotates at first, and then rotates slightly clockwise. This is consistent with previous experimental and numerical results [42,43,48,50]. But after $t>0.016$, the rotation shifting phenomenon happens and the particle rotates counterclockwise, as shown in Fig. 6(a). This rotation shifting event also happens several times in the whole time framework demonstrated in Fig. 6(b). Its mechanism is associated with the hydrodynamic interactions between the particle, the surrounding fluid, and the wall, which needs to be further explored in future work. The angular velocity of the particle increases fast at first, but then decreases semiperiodically and fluctuates when the particle settles and moves away from the left wall.

Figure 7 shows the vorticity contour and the particle position as well as the rotation direction at different times when the particle settles near the wall. The typical sedimentation dynamics of a single particle near one wall in a channel with Newtonian fluid are reproduced. Compared with the particle settling initially from the middle of the flow field, the vortex shedding occurs early when the particle settles initially near one wall. These alternately shedding vertical structures are expected to be responsible for some microcosmic phenomena, such as rotation shifting. The trajectory of particle sedimentation and its orientation are also depicted in Fig. 7(h). One can observe all the prominent phenomena stated above, such as the lateral migration, the anomalous rolling, and the rotation shifting. This also indicates that the proposed multidirect forcing scheme is reliable to simulate flows immersed with moving particles with full-scale solutions.

V. SUMMARY

In this study, a multidirect forcing scheme is presented to calculate the hydrodynamic interactions between the rigid solid boundary and the Newtonian fluid based on the immersed boundary method. By applying this scheme, the no-slip condition near the immersed solid boundary is able to be efficiently satisfied. It is validated by simulations of the flows around a stationary circular disc at different Reynolds numbers and the free sedimentation of a particle. The predicted data agree well with previous experimental and numerical results. This method is also applied to study particle sedimentation near a vertical wall and some microcosmic phenomena, such as the rotation shifting, the lateral migration, and the anomalous rolling, are successfully observed. This scheme is simple but efficient, and only one parameter, the time of multidirect forcing, should be determined in the coupling process.

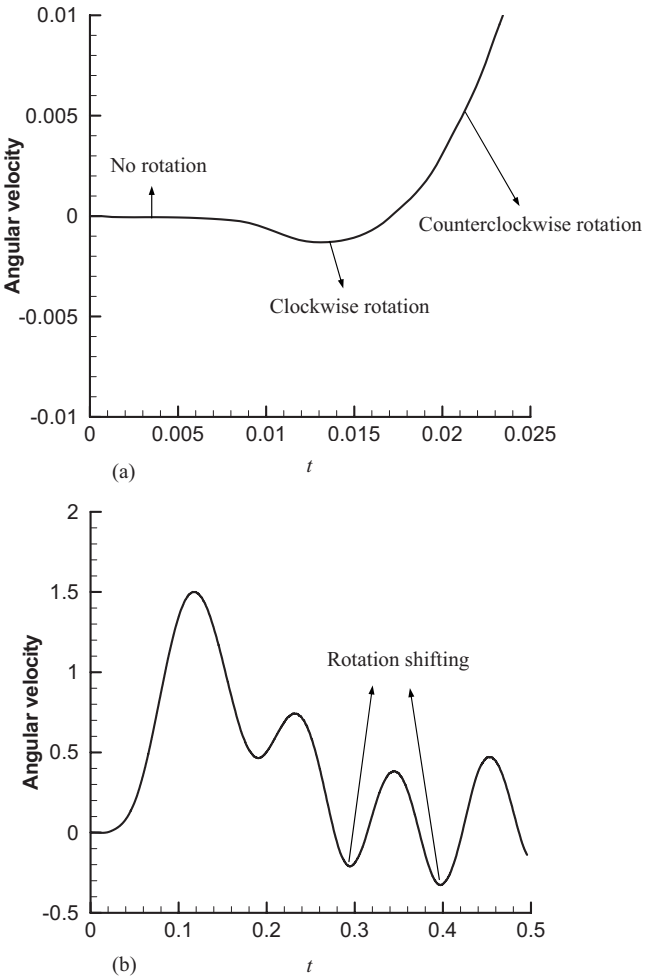

FIG. 6. Time history of the particle angular velocity for particle sedimentation near a wall under the condition of particle density $\rho_P=1.5$ and fluid viscosity $\mu=0.01$; (a) Very beginning time framework (b). Whole time framework.

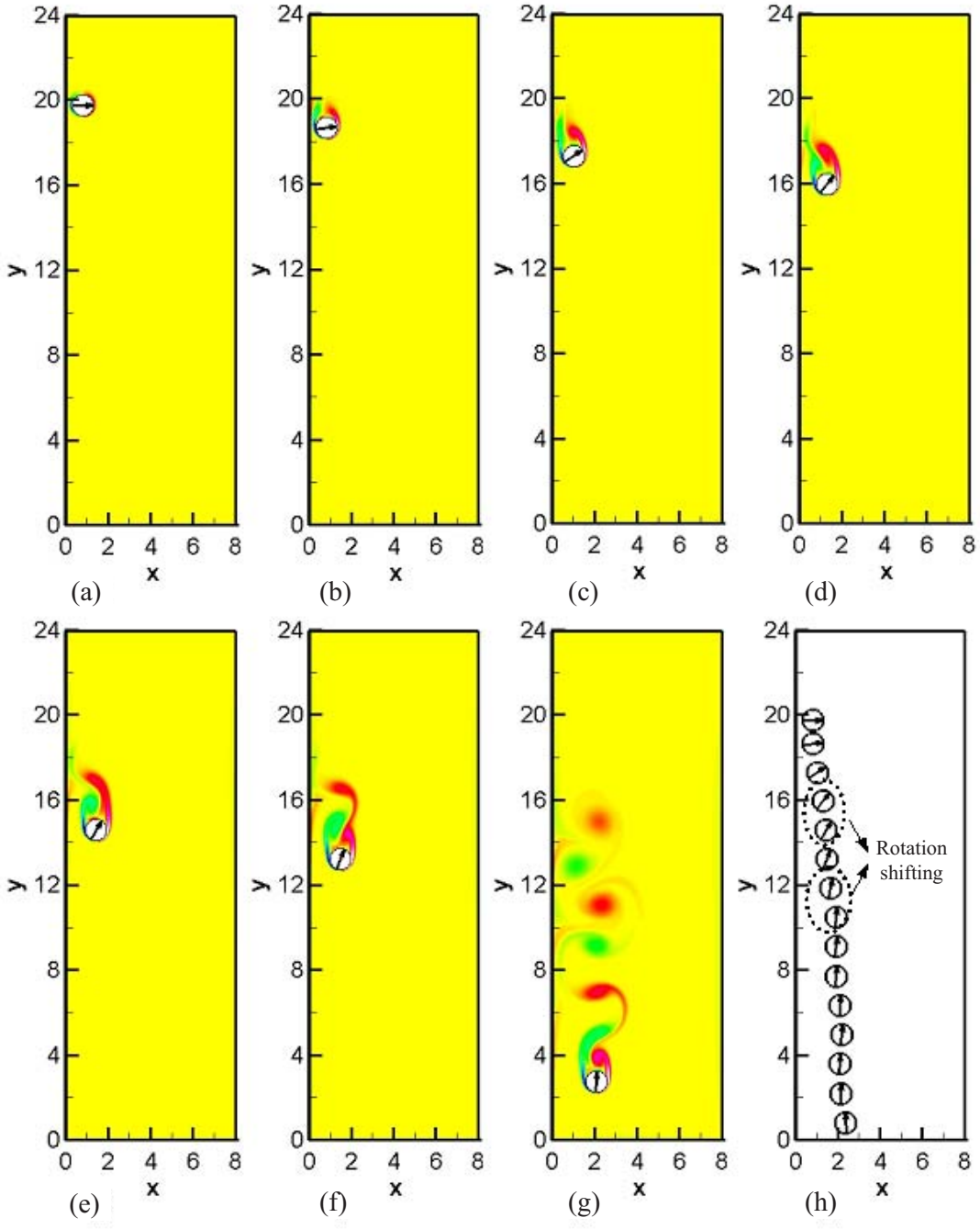

FIG. 7. (Color online) Vorticity contour and particle position as well as rotation direction during particle sedimentation near the wall under the condition of particle density $\rho_P=1.5$ and fluid viscosity $\mu=0.01$. (a) $t=0.0326$, (b) $t=0.0822$, (c) $t=0.1229$, (d) $t=0.1574$, (e) $t=0.1896$, (f) $t=0.2206$, (g) $t=0.4485$, (h) trajectory of particle sedimentation and its orientation.

ACKNOWLEDGMENTS

This work was supported by the National Natural Science Foundation of China (Grant Nos. 50776080 and 50736006), for which the authors we are grateful. The authors also ap preciate the insightful and detailed comments from the anonymous reviewers of the paper.

[1] C. Crowe, M. Sommerfeld, and Y. Tsuji, *Multiphase Flows with Droplets and Particles* (CRC, Boca Raton, FL, 1998).
[2] R. Nathan, G. G. Katul, H. S. Horn, S. M.Thomas, R. Oren, R. Avissar, S. W. Pacala, and S. A. Lein, Nature (London) **418**, 409 (2002).
[3] G. Falkovich, A. Fouxon, and M. G. Stepanov, Nature (London) **419**, 151 (2002).
[4] T. Elperin, N. Kleeorin, and I. Rogachevskii, Phys. Rev. Lett. **76**, 224 (1996).
[5] E. Balkovsky, G. Falkovich, and A. Fouxon, Phys. Rev. Lett. **86**, 2790 (2001).
[6] T. Elperin, N. Kleeorin, V. S. Lvov, I. Rogachevskii, and D. Sokoloff, Phys. Rev. E **66**, 036302 (2002).
[7] J. Bec, K. Gawedzki, and P. Horvai, Phys. Rev. Lett. **92**, 224501 (2004).
[8] K. Luo, J. R. Fan, and K. F. Cen, Phys. Rev. E **75**, 046309 (2007).
[9] H. H. Hu, Int. J. Multiphase Flow **22**, 335 (1996).
[10] H. Hu, N. Patankar, and N. Zhu, J. Comput. Phys. **169**, 427 (2001).
[11] A. J. C. Ladd, Phys. Rev. Lett. **70**, 1339 (1993).
[12] A. J. C. Ladd, Phys. Rev. Lett. **76**, 1392 (1996).
[13] W. Kalthoff, S. Schwarzer, and H. J. Herrmann, Phys. Rev. E **56**, 2234 (1997).
[14] R. Glowinski, T. W. Pan, T. I. Hesla, and D. D. Joseph, Int. J. Multiphase Flow **25**, 755 (1999).
[15] R. Kutteh, Phys. Rev. E **69**, 011406 (2004).
[16] M. Sussman, P. Smereka, and S. Osher, J. Comput. Phys. **114**, 146 (1994).
[17] G. Tryggvason, B. Bunner, A. Esmaelli, and N. Al-Rawahi, W, J. Comput. Phys. **169**, 708 (2001).
[18] C. S. Peskin, J. Comput. Phys. **10**, 252 (1972).
[19] R. Mittal and G. Iaccarino, Annu. Rev. Fluid Mech. **37**, 239 (2005).
[20] D. Goldstein, R. Handler, and L. Sirovich, J. Comput. Phys. **105**, 354 (1993).
[21] K. Hofler and S. Schwarzer, Phys. Rev. E **61**, 7146 (2000).
[22] T. Kajishima and S. Takiguchi, Int. J. Heat Fluid Flow **23**, 639 (2002).
[23] Y. Nakayama and R. Yamamoto, Phys. Rev. E **71**, 036707 (2005).
[24] C. Yang and Z. S. Mao, Phys. Rev. E **71**, 036704 (2005).
[25] E. A. Fadlun, R. Verzicco, P. Orlandi, and J. Mohd-Yusof, J. Comput. Phys. **161**, 35 (2000).
[26] J. Mohd-Yusof, annual research briefs, Center for Turbulence Research, Stanford University, 1997.
[27] S. K. Lele, J. Comput. Phys. **103**, 16 (1992).
[28] A. Jameson and W. Schmidt, Comput. Methods Appl. Mech. Eng. **51**, 467 (1985).
[29] A. L. F. L. E. Silva, A. Silveira-Neto, and J. J. R. Damasceno, J. Comput. Phys. **189**, 351 (2003).
[30] B. E. Griffith and C. S. Peskin, J. Comput. Phys. **208**, 75 (2005).
[31] M. Uhlmann, J. Comput. Phys. **209**, 448 (2006).
[32] I. Orlanski, J. Comput. Phys. **21**, 251 (1976).
[33] E. M. Saiki and S. Biringen, J. Comput. Phys. **123**, 450 (1996).
[34] M. C. Lai and C. S. Peskin, J. Comput. Phys. **160**, 705 (2000).
[35] S. W. Su, M. C. Lai, and C. A. Lin, Comput. Fluids **36**, 313 (2007).
[36] S. Xu and Z. J. Wang, J. Comput. Phys. **216**, 454 (2006).
[37] D. J. Triton, J. Fluid Mech. **6**, 547 (1959).
[38] C. H. Williamson, Annu. Rev. Fluid Mech. **28**, 477 (1996).
[39] D. C. Wan and S. Turek, J. Comput. Appl. Math. **203**, 561 (2007).
[40] S. Y. Tee, P. J. Mucha, L. Cipelletti, S. Manley, M. P. Brenner, P. N. Segre, and D. A. Weitz, Phys. Rev. Lett. **89**, 054501 (2002).
[41] J. J. Lietor-Santos, A. Fernandez-Nieves, and M. Marquez, Phys. Rev. E **74**, 051404 (2006).
[42] L. E. Becker, G. H. McKinley, and H. A. Stone, J. Non-Newtonian Fluid Mech. **63**, 201 (1996).
[43] P. Singh and D. D. Joseph, J. Non-Newtonian Fluid Mech. **94**, 179 (2000).
[44] A. J. C. Ladd, Phys. Rev. Lett. **88**, 048301 (2002).
[45] E. Kuusela, J. M. Lahtinen, and T. Ala-Nissila, Phys. Rev. E **69**, 066310 (2004).
[46] P. Ganatos, R. Pfeffer, and S. Weinbaum, J. Fluid Mech. **99**, 755 (1980).
[47] D. J. Jeffrey and Y. Onishi, Q. J. Mech. Appl. Math. **34**, 129 (1981).
[48] Y. J. Liu, J. Nelson, J. Feng, and D. D. Joseph, J. Non-Newtonian Fluid Mech. **50**, 305 (1993).
[49] H. Binous and R. J. Phillips, J. Non-Newtonian Fluid Mech. **85**, 63 (1999).
[50] D. D. Joseph, Y. J. Liu, M. Poletto, and J. Feng, J. Non-Newtonian Fluid Mech. **54**, 45 (1994).